

Remapping simulated halo catalogues in redshift space

A. J. Mead^{1*} and J. A. Peacock¹

¹*Institute for Astronomy, University of Edinburgh, Royal Observatory, Blackford Hill, Edinburgh EH9 3HJ*

Accepted 2014 September 18. Received 2014 September 18; in original form 2014 August 5

ABSTRACT

We discuss the extension to redshift space of a rescaling algorithm, designed to alter the effective cosmology of a pre-existing simulated particle distribution or catalogue of dark matter haloes. The rescaling approach was initially developed by Angulo & White and was adapted and applied to halo catalogues in real space in our previous work. This algorithm requires no information other than the initial and target cosmological parameters, and it contains no tuned parameters. It is shown here that the rescaling method also works well in redshift space, and that the rescaled simulations can reproduce the growth rate of cosmological density fluctuations appropriate for the target cosmology. Even when rescaling a grossly non-standard model with $\Lambda = 0$ and zero baryons, the redshift-space power spectrum of standard Λ CDM can be reproduced to about 5% error for $k < 0.2 h \text{ Mpc}^{-1}$. The ratio of quadrupole-to-monopole power spectra remains correct to the same tolerance up to $k = 1 h \text{ Mpc}^{-1}$, provided that the input halo catalogue contains measured internal velocity dispersions.

Key words: cosmology: theory – large-scale structure of universe

1 INTRODUCTION

Numerical simulations are now an essential standard tool in the analysis and interpretation of cosmological surveys. Modern examples of which deliver high statistical power and are seeking to measure cosmological parameters with ever-increasing precision, thus requiring a corresponding rise in the care with which observational selection effects are treated. Practical survey complications are inevitably encountered to some extent, such as difficulty in obtaining spectra for adjacent objects in multiplexed spectroscopic surveys, and these are most robustly treated via Monte Carlo: analysis of a simulated mock dataset where the underlying cosmological parameters are known. This approach is increasingly deployed in order to verify the robustness of parameter estimates, or to identify and eliminate small residual biases. It can be witnessed in action in measurements of Baryon Acoustic Oscillations (BAO) in the galaxy distribution (e.g. Anderson et al. 2014) or in redshift-space distortions of galaxy clustering (e.g. Samushia et al. 2013; de la Torre et al. 2013).

Such studies also require the generation of large libraries of simulations. An ensemble of mock datasets is always required for a given cosmology, simply in order to generate an estimate of the data covariance matrix; this is used on the assumption of a Gaussian error distribution to calculate the likelihood of a given hypothetical model with respect to

the data. In order for the final parameter constraints to be meaningful (small ‘errors on the errors’), the data covariance matrix itself must be precisely measured. This can require an ensemble of ~ 1000 simulations – or significantly more if the size of the dataset under study is sufficiently large (Taylor et al. 2013).

But the size of the numerical challenge is greatly increased if we accept that, in principle, a new ensemble of simulations is required for each new cosmological model under study. Moreover, mock *galaxy* data are required, so in principle a galaxy formation code must be run as part of each simulation. The latter issue can be dealt with rapidly using halo occupation distribution (HOD) models (e.g. Zheng et al. 2005), reducing the problem to one of obtaining catalogues of dark-matter haloes for the model under study. A way to speed up this basic generation of dark-matter simulations was presented by Angulo & White (2010; hereafter AW10). They showed that it was possible to rescale an N -body particle distribution so that the results closely approximated the output of a simulation with a different set of cosmological parameters.

In Mead & Peacock (2014; hereafter MP14) we showed that the AW10 method could be applied directly to halo catalogues, yielding a mass function and power spectrum of haloes that were well matched to the target cosmology following rescaling. In fact, this approach is capable of yielding more accurate results, since it retains the mass-dependent halo bias relation and can incorporate a cosmology dependence of halo concentrations. Moreover, this method has

* E-mail: am@roe.ac.uk

a major practical advantage in terms of data compression: halo catalogues take up several orders of magnitude less storage than the raw particle data, and thus it is often the case that only the halo catalogue is made public (or even stored) by major simulation projects such as that of Rasera et al. (2010).

In MP14 we showed that these methods worked well on haloes in real space; in this paper we extend our approach to redshift space. The algorithm presented here consists of the following steps: (a) Initially the length and time units in the original halo catalogue are rescaled, in order to match the halo mass function, exactly as in the original AW10 algorithm. (b) In MP14 we showed that the particle or halo distribution itself may be used to compute the linear displacement field, from which we modify particle or halo positions and velocities so that they reproduce the correct large-scale clustering in the target cosmology. Eisenstein et al. (2007) showed how to recreate the displacement fields via the overdensity field, and Padmanabhan et al. (2012) used a variant of this approach to improve the sharpness of the BAO feature in BOSS data. (c) Finally, we modify the halo internal physical and velocity structure directly – by ‘reconstituting’ the density profiles around haloes so that they have the correct sizes and internal structure for the target cosmology. In this way, the rescaled velocity field contains both the linear velocities that contribute coherent redshift-space distortions (Kaiser 1987) and the post-linear effects that cause the ‘fingers-of-God’ (FOG) distortion.

Our paper is set out as follows: In Section 2 we briefly review the AW10 and MP14 algorithms and explain the extensions required to get good results in redshift space. We discuss the cosmology dependence of the internal physical and velocity structure of haloes. In Section 3 we describe our simulations and our methods for generating halo catalogues. In Section 4 we discuss our conventions and method for generating power spectra in redshift space. In Section 5 we show results for the full redshift-space power spectrum as well as the monopole and quadrupole moments of this. Results are presented for matter, haloes, and particles within haloes, and we show that an accurate recovery of the growth rate may be made from the rescaled distributions. Finally we sum up in Section 6.

2 METHOD

2.1 Overview of rescaling

We begin with a summary of the main features of the AW10 method and the MP14 extension. Quantities in the target cosmology are denoted with primes while the original quantities are unprimed. The original simulation output at redshift z , in a box of size L , is rescaled to a target simulation at redshift z' , in a box of size $L' = sL$. For a given z' , s and z are chosen so as to minimize the difference in $\sigma^2(R)$ (the *linear-theory* variance in density averaged over spheres of comoving radius R) between the two cosmologies. The following cost function is convenient:

$$\delta_{\text{rms}}^2(s, z | z') = \frac{1}{\ln(R'_2/R'_1)} \int_{R'_1}^{R'_2} \frac{dR}{R} \left[1 - \frac{\sigma(R/s, z)}{\sigma'(R, z')} \right]^2, \quad (1)$$

with $R' = sR$. R_1 and R_2 are chosen so as to relate to the physical scale of the least and most massive haloes in the original simulation via

$$M = \frac{4}{3} \pi R^3 \bar{\rho}, \quad (2)$$

where $\bar{\rho}$ is the mean comoving density. This approach is taken because the halo mass function is approximately universal when expressed in terms of the variable $\nu = \delta_c/\sigma(R)$ where $\delta_c \simeq 1.686$ (e.g. Press & Schechter 1974; Sheth & Tormen 1999; Sheth et al. 2001), and because the statistics of the nonlinear density field are driven by the mass function of haloes. In detail, the mass function displays deviations from universality at up to around the 10% level, so more accurate results might be obtained by directly matching theoretical predictions for a non-universal mass function (e.g. Lukić et al. 2007; Reed et al. 2007; Tinker et al. 2008). We have chosen not to do this because these mass functions are tuned to specific cosmological parameters and we are interested in quite broad shifts in cosmology in this work. Similarly, one might minimize the difference in $\nu(M) = \delta_c/\sigma(M)$ where δ_c could be taken to vary with cosmology. For standard models, these variations in δ_c are negligible (e.g. Eke et al. 1996; Lacey & Cole 1993; Percival 2005), but large variations in δ_c are a feature of some modified gravity models (e.g. Schmidt et al. 2009; Li & Efstathiou 2012), owing to screening mechanisms.

In order to conserve mass the scaling in length units simultaneously implies a scaling in mass:

$$M' = s^3 \frac{\Omega'_m}{\Omega_m} M \equiv s_m M. \quad (3)$$

Note that we use units of h^{-1} Mpc for length and $h^{-1} M_\odot$ for mass and the necessary factors of h are included in the scalings.

Additionally the dimensionless velocity units of the simulation must be conserved before and after scaling (see AW10; MP14) which implies a scaling in bulk velocities of particles or haloes such that

$$\mathbf{v}' = s \frac{H'(a') f'_g a'}{H(a) f_g a} \mathbf{v}, \quad (4)$$

where H is the Hubble parameter at the epoch in question; $f_g \equiv d \ln g / d \ln a$ is the logarithmic growth rate; $g(a)$ is the linear theory growth function; and a is the scale factor.

Following scaling in s and z , the two cosmologies should have similar nonlinear power spectra; but the linear power on large scales will in general not be matched. This difference can be corrected for by using the approximation of Zel’dovich (1970; hereafter ZA) to perturb the particle or halo positions using the displacement field: the phase of each mode of the large-scale displacement field is preserved, but the amplitude is altered to match the target power spectrum. The displacement field \mathbf{f} is defined so as to move particles from their initial Lagrangian positions \mathbf{q} to their comoving Eulerian positions \mathbf{x} :

$$\mathbf{x} = \mathbf{q} + \mathbf{f}. \quad (5)$$

At linear order the displacement field is related to the matter over-density δ via

$$\delta = -\nabla \cdot \mathbf{f}, \quad (6)$$

which in Fourier space is

$$\mathbf{f}_{\mathbf{k}} = -i \frac{\delta_{\mathbf{k}}}{k^2} \mathbf{k} . \quad (7)$$

If the displacement field in the original simulation is known, then an additional displacement can be specified in Fourier space to reflect the differences in the linear matter power spectra between the two cosmologies:

$$\delta \mathbf{f}'_{\mathbf{k}'} = \left[\sqrt{\frac{\Delta'^2_{\text{lin}}(k', z')}{\Delta^2_{\text{lin}}(sk', z)}} - 1 \right] \mathbf{f}'_{\mathbf{k}'} . \quad (8)$$

where Δ^2 is the power spectrum in the form of fractional variance in density per $\ln k$, and \mathbf{f}' is the linear displacement field after the input simulation has been scaled.

The particle or halo positions in the original simulation can be used to estimate the overdensity field via equation (7). To derive the overdensity of matter from the halo overdensity field, δ_{H} , must be debiased, respecting the relation

$$\delta_{\text{H}} = b(M)\delta ; \quad (9)$$

in practice, we use the bias relations of Sheth & Tormen (1999). We then define a number-weighted effective bias for all haloes:

$$b_{\text{eff}} = \frac{\int_{\nu_{\text{min}}}^{\nu_{\text{max}}} d\nu b(\nu) f(\nu) / m(\nu)}{\int_{\nu_{\text{min}}}^{\nu_{\text{max}}} d\nu f(\nu) / m(\nu)} , \quad (10)$$

where $f(\nu) d\nu$ is the fraction of the total density contributed by haloes in the range $d\nu$. For very low-mass haloes $b(M) < 1$ and the method could in principle yield an unphysical negative mass density. In practice, this method is of interest for large-volume simulations where haloes of extremely low mass are not resolved, and we always find $b_{\text{eff}} > 1$. Negative densities can always be avoided either by using something more sophisticated than a linear biasing relation, or by using haloes only above a certain mass to recreate the overdensity field.

Equation (7) is only valid for the linear components of both fields, so in practice the reconstructed δ must be smoothed with a window of width the nonlinear scale R_{nl} to remove the nonlinear components. To do this we use a Gaussian filter

$$F(k) = e^{-k^2 R_{\text{nl}}^2 / 2} , \quad (11)$$

where $\sigma(R_{\text{nl}}, z) = 1$. Then equation (7) can be used to estimate the linear displacement field in Fourier space and particles can be displaced differentially in order to account for the differing linear power spectra:

$$\mathbf{x}'' = \mathbf{x}' + \delta \mathbf{f}' , \quad (12)$$

where the double dash indicates positions after this displacement has been applied. As noted in MP14, haloes are biased tracers of the density field and their effective displacement fields must therefore also be biased. Thus $\mathbf{f}_{\text{H}} = b(M)\mathbf{f}$ for each halo. In MP14, good results for the rescaled halo power spectrum were in general *not* obtained unless a biased displacement field was used.

The ZA also allows residual differences in linear velocities to be corrected on a mode-by-mode basis. In the ZA the peculiar velocity field ($\mathbf{v} \equiv a\dot{\mathbf{x}}$) is related to the displacement field by $\mathbf{v} = aHf_{\text{g}}\mathbf{f}$ and additional differential changes to the peculiar velocities of particles or haloes are then given by

$$\delta \mathbf{v}'_{\mathbf{k}'} = a'H'f'_{\text{g}} \left[\sqrt{\frac{\Delta'^2_{\text{lin}}(k', z')}{\Delta^2_{\text{lin}}(sk', z)}} - 1 \right] \mathbf{f}'_{\mathbf{k}'} . \quad (13)$$

Note that, in contrast to the displacement field case, the halo velocities are unbiased: the equivalence principle requires haloes of all masses in a given region to share a common large-scale velocity. The final velocities after the displacement field step are then

$$\mathbf{v}'' = \mathbf{v}' + \delta \mathbf{v}' . \quad (14)$$

At this stage the linear power and mass function should be very close to the desired target. According to the halo model (e.g. Peacock & Smith 2000; Seljak 2000; Cooray & Sheth 2002), matching the mass function should also yield the correct quasi-linear clustering. Note that the rescaling method naturally includes effects such as halo exclusion (Smith, Desjacques, & Marian 2011) because it is based on rescaling an exact N -body calculation. However, the highly nonlinear part of the power spectrum is influenced by the internal structure of haloes, and this will also change if the cosmology is altered (e.g. Navarro et al. 1997; Bullock et al. 2001; Dooley et al. 2014). Such effects will alter the mass distribution defined by the haloes, and will also be important in producing mock galaxy catalogues using HOD methods. Here, a given halo is typically assigned a central galaxy and a number of satellite galaxies that are taken to trace the density profile. It is therefore necessary to consider how the internal structure of haloes should be rescaled. Note that such an adjustment is not part of the original AW10 method, which is a further advantage of the current approach.

AW10 was first applied directly to galaxy catalogues by Ruiz et al. (2011). Differences in galaxy formation between cosmological models have been studied using this method by Guo et al. (2013) and the cosmological constraints one can derive from differences in galaxy clustering are discussed by Simha & Cole (2013) (who used sub-halo abundance matching to populate rescaled catalogues with galaxies). In all cases only small scales were investigated and the large-scale ZA correction was not applied to the halo distribution. MP14 was the first work to successfully apply the ZA correction when working directly with a halo catalogue.

2.2 Rescaling halo properties

2.2.1 Halo catalogues

Beyond positions, velocities and masses of haloes, there are a number of other properties that may plausibly be stored in a halo catalogue (see Table 1). Halo radial density profiles have been shown to be accurately approximated on average by the ‘NFW’ profile of Navarro, Frenk, & White (1997):

$$\rho(r) = \frac{\rho_{\text{N}}}{(r/r_{\text{s}})(1+r/r_{\text{s}})^2} , \quad (15)$$

where r_{s} is a scale radius and ρ_{N} is a normalization to obtain the correct halo mass. Although subsequent work (Moore et al. 1999; Merritt et al. 2005; Merritt et al. 2006) showed this form to be imperfect at small r , it will suffice for our present purpose: mock galaxies are either central at $r = 0$ exactly, or satellites that tend to be found around r_{s} , where the NFW approximation is good. The density profile

is truncated at the virial radius r_v , which will depend on the exact definition of a halo; this can be measured directly or inferred from the halo mass:

$$r_v = \left(\frac{3M}{4\pi\Delta_v\bar{\rho}} \right)^{1/3}, \quad (16)$$

where Δ_v is the average density of a halo with respect to the background matter density. We adopt the common value of 178, justified by the near-universality of the halo mass function when defining haloes via the friends-of-friends algorithm with a cosmology-independent linking length.

The density profile is therefore fully specified via a value for r_s or alternatively for the halo concentration $c = r_v/r_s$. There are many suggested relations for determining the concentration as a function of cosmological parameters (e.g. Navarro et al. 1997; Eke et al. 2001; Bullock et al. 2001; Neto et al. 2007). We adopt the relations of Bullock et al. (2001) because they are couched in term of physical quantities such as halo formation time, rather than being empirical fitting functions that apply only to a limited range of models.

Apart from virial radii and concentration, additional quantities that may be stored with a halo catalogue are the halo velocity dispersion, σ_v , and the eigenvalues, λ^2 , and eigenvectors, \mathbf{w} , of the moment of inertia tensor, which gives a measure of halo asphericity:

$$I_{ij} = \sum_{k=1}^N (x_{k,i} - \bar{x}_i)(x_{k,j} - \bar{x}_j). \quad (17)$$

Here \mathbf{x}_k is position of the k^{th} halo particle with halo centre-of-mass (CM) position $\bar{\mathbf{x}}$, $k \in \{1, \dots, N\}$ and there are N particles in each halo and $i, j \in \{1, 2, 3\}$ and label coordinates. Diagonalizing this tensor provides the axial ratios of the halo (via the eigenvalues) and the orientation of the halo (via the eigenvectors). In practice, we use a minimum size of $N = 100$ particles for this estimation.

We now discuss how each of these may be scaled: Measured concentrations may be scaled by a ratio of theoretical predictions taken from a relation such as Bullock et al. (2001); this corrects the mean relation, and implicitly assumes that the fractional scatter in concentrations of individual haloes has no strong cosmology dependence. Virial radii will be scaled by a factor of s because the virial overdensity criterion is independent of cosmology. For the NFW profile, and assuming isotropic orbits, the halo velocity dispersion is

$$\sigma_v^2 = \frac{GM}{3r_v} \frac{c[1 - 1/(1+c)^2 - 2\ln(1+c)/(1+c)]}{2[\ln(1+c) - c/(1+c)]^2}, \quad (18)$$

which would give the scaling a mild concentration dependence. We chose not to use this more complicated formula for this initial investigation, adopting the simple approximation of

$$\sigma_v^2 \simeq \frac{GM}{3r_v}, \quad (19)$$

from which a scaling factor for σ_v of $s\sqrt{\Omega'_m/\Omega_m}$ follows. The difference in σ_v between equations (18) and (19) is only $\simeq 10\%$ for concentrations of interest in this work ($c < 10$). We do not attempt to solve the Jeans equation for the velocity dispersion as a function of radius (which would be

possible given assumptions about orbital anisotropy). The limitations of halo scaling in redshift space that we uncover below would not be removed by such complications. The scalings we use in practice are summarized in Table 1.

2.2.2 Reconstitution of haloes

Given a hypothesis for the the density profile of a given halo, one may undertake *reconstitution* of the halo, either to recreate the dark-matter particles of which the halo is composed, or to populate it with mock galaxies. In the former case, one can use the NFW profile to place particles at random in order to sample the density (ignoring subhaloes). The boundary of a halo can either be taken to be given by r_v according to equation (16) with a concentration given by a relation such as Bullock et al. (2001) or these can be taken from rescaled stored values. Haloes can then be assigned a velocity dispersion via either equation (18) or (19). The simplest approach is then to take the velocity components to be Gaussian distributed (see Kazantzidis et al. 2004; Wojtak et al. 2005 for limitations); we examined the approximation of Gaussian internal halo velocities in testing and found it to be accurate for our particular definition of haloes in our simulations (see section 3).

If desired, aspherical reconstitution can be achieved by distorting the halo particle distribution once it has been generated by the spherical halo reconstitution process described above. If the square roots of the eigenvalues are λ_1, λ_2 and λ_3 then each coordinate of the particles in the reconstituted halo in the CM frame, \mathbf{y} , is modified according to

$$y_i \rightarrow 3\lambda_i y_i / (\lambda_1 + \lambda_2 + \lambda_3), \quad (20)$$

where $i \in \{1, 2, 3\}$. We also considered the prescription $y_i \rightarrow \lambda_i y_i / (\lambda_1 \lambda_2 \lambda_3)^{1/3}$ etc. but found this to work less well in recovering the shapes of aspherical haloes. The relative to CM position vector of each halo particle is then rotated by the inverse matrix of eigenvectors in order to orient the halo correctly.

2.2.3 Restructuring halo particles

Given access to the full particle distribution, two options are available to match the haloes in the target cosmology; one could either remove haloes from the rescaled particle distribution entirely, replacing them with reconstituted haloes in the manner described above – a method we call ‘regurgitation’. Alternatively the haloes can be identified in the scaled distribution and reshaped to account for the different cosmology – a method we call ‘restructuring’. Again we point out that it would be difficult to implement the biased displacement field for haloes if working from a particle distribution, and so the $b(M)$ relation will not be correctly reproduced in this case.

To restructure haloes in a rescaled particle distribution one can proceed as follows: The amount of mass enclosed by an NFW profile at a radius r is given by

$$M_{\text{enc}}(r) = M \frac{\mu(r/r_s)}{\mu(c)} \equiv f(r)M, \quad (21)$$

where

$$\mu(x) = \ln(1+x) - \frac{x}{1+x}. \quad (22)$$

quantity	symbol	scaling	comments
Positions	\mathbf{x}	s	Additionally use equation (8) for linear displacements
Velocities	\mathbf{v}	$s H' f'_g a' / H f_g a$	Additionally use equation (13) for linear velocities
Particle or halo mass	M	$s^3 \Omega'_m / \Omega_m$	–
Virial radius	r_v	s	Although this depends on how c is defined
Halo concentration	c	$c'_{\text{th}} / c_{\text{th}}$	c_{th} (theoretical) computed from any $c(M)$ relation
Halo velocity dispersion	σ_v	$s \sqrt{\Omega'_m / \Omega_m}$	Alternatively use equation (18) with c dependence
Inertia tensor eigenvalues	λ^2	s^2	–
Normalized inertia tensor eigenvectors	\mathbf{w}	–	No scaling because they are normalized

Table 1. Scalings for various quantities that may be contained in a halo catalogue.

Haloes can be reshaped by the ratio of mass enclosed at a radius r from the halo centre in each case. A scaled particle originally at r' should be moved to r'' , given by

$$r'' = f''^{-1}[f'(r')], \quad (23)$$

where f^{-1} indicates the inverse function. f'' will be the value of f in the target cosmology whereas f' will be the value in the original cosmology *after it has been scaled*. Particle positions relative to the CM can then be reassigned via

$$\mathbf{y}'' = \frac{r''}{r'} \mathbf{y}', \quad (24)$$

so that they end up with the correct interior distribution for haloes in the new cosmology, but allowing the haloes to maintain any asphericity they may have had. This also means that the haloes retain any dispersion in structure and environmental dependence that they may have had in the original simulation. This requires the input of a $c(M)$ relation, and as before we adopt the relations of Bullock et al. (2001). For ‘real’ haloes it is possible for particles to be outside the official virial radius (calculated from equation 16) for haloes defined with a friends-of-friends (FOF) algorithm, which is used in this work. Using equation (24) is still possible in this case but $f > 1$ for these particles.

Halo particle velocities, \mathbf{u} , relative to the CM velocity, can be reassigned via

$$\mathbf{u}'' = \frac{\sigma''_v}{\sigma'_v} \mathbf{u}', \quad (25)$$

with σ_v taken from either equation (19) or (18). This should make the halo velocity dispersion appropriate for the new cosmology whilst maintaining the dispersion and environmental dependence in the dispersion relation for haloes of a given mass.

3 SIMULATIONS

We now show the operation of halo rescaling in redshift space, using the same matched set of simulations, with corresponding halo catalogues, as in MP14. The simulation parameters are given in Table 2. The target Λ CDM simulation is a WMAP1-style cosmology (Spergel et al. 2003) run with the same transfer function as that of the Millennium Simulation (Springel et al. 2005) which was generated using CMBFAST (Seljak & Zaldarriaga 1996). The input simulation τ CDM is a flat matter-only simulation run with a DEFW transfer function (Davis et al. 1985) tuned to have a simi-

lar spectral shape to that of the Millennium Simulation. The historical popularity of τ CDM models is explained in MP14.

We take this extreme approach (no Λ or baryons) in order to see how well rescaling can work over any range of models of conceivable interest. For smaller variations in cosmological parameters, we may expect that the results will be correspondingly more accurate. Additionally; any practical application of this method would scale to a variety of cosmological models from a *single* parent simulation of high σ_8 , such that it explored a large range of fluctuation amplitudes. In this case scalings to standard models are likely to come from the $\Omega_m \simeq 1$ regime of the parent simulation anyway, even if it is Λ CDM.

Initial conditions were generated at $z_i = 199$, using a glass initial load of 512^3 particles, created using the N-GenIC code. The simulations were run using the cosmological N -body code **Gadget-2** of Springel (2005). As in MP14, we used the same phases for the Fourier modes in the target and original simulations, so that the approximate and exact target halo fields can be compared visually, and not purely at the level of power spectra. This also allows us to analyse the results of the rescaling without the added complication of cosmic variance.

Initially, we ran the original simulation to $z = 0$ in a box of size L ; but having computed the best scaling parameters (s, z) to match the target simulation, we then re-ran the original simulation to generate an output at exactly redshift z . In practice one would need to interpolate particle positions between simulation outputs near to redshift z if one was interested in particles, or constrain the scaling redshift to be one of a set of z (close to the best fit) for which one already had an output. This would be necessary in the case of halo catalogues because halo mergers mean that it is not straightforward to interpolate haloes between catalogues at different epochs. We also ran a simulation of the target cosmology to $z' = 0$ in a box of size $L' = sL$, using the same mode phases and amplitudes for the displacement fields so that structures in the target and scaled simulations could be compared directly without the added complication of cosmic variance.

Halo catalogues were generated with the public FoF code www-hpcc.astro.washington.edu/tools/fof.html, using a linking length of $b = 0.2$ times the mean inter-particle separation. No attempt was made to reject unbound particles.

For our simulations the best-fit scaling parameters are summarised in Table 3. The match to the mass function produced by this scaling was shown in MP14 and is good

Simulation	L	Ω_m	Ω_Λ	Ω_b	h	σ_8	n_s	Γ
Λ CDM	$780 h^{-1} \text{ Mpc}$	0.25	0.75	0.045	0.73	0.9	1	–
τ CDM	$500 h^{-1} \text{ Mpc}$	1	0	–	0.5	0.8	1	0.21

Table 2. Cosmological parameters for our simulations. As a target we use a Λ CDM model with a WMAP1 type cosmology and as an input model we simulate a CDM-only model with a DEFW (Davis et al. 1985) spectrum having a similar spectral shape ($\Gamma = 0.21$) to that of the Λ CDM model but lacking a BAO feature. Each simulation was run with $N^3 = 512^3$ particles, gravitational forces were softened at $20 h^{-1} \text{ kpc}$ and initial conditions generated using **N-GenIC** on an initial glass load at a starting redshift $z_i = 199$.

Original	Target	z	z'	s	M_1	M_2	s_m	k'_{nl}	b_{eff}
τ CDM	Λ CDM	0.22	0	1.56	$2.58 \times 10^{13} h^{-1} M_\odot$	$7.19 \times 10^{15} h^{-1} M_\odot$	0.95	$0.15 h \text{ Mpc}^{-1}$	1.57

Table 3. Best fit scaling parameters s and z' for scaling between our original τ CDM model and our target Λ CDM model together with the mass range of haloes in the original simulation ($M_1 \rightarrow M_2$) and the non-linear wave number in the target cosmology k_{nl} .

only to the 10% level across all masses, despite $\sigma(R)$ being matched to within 1% across all scales relevant to these haloes (Fig. 1 of MP14). A similar level of disagreement in the measured mass function was found in AW10 (their Fig. 7) in converting between WMAP1 and WMAP3 cosmologies and plausibly reflects non-universality of the mass function.

4 POWER SPECTRA

4.1 Estimation

In order to measure power spectra in redshift space, the particles are moved to their redshift-space positions. We use the distant-observer approximation, and move particles to redshift space positions \mathbf{s} , via

$$\mathbf{s} = \mathbf{x} + \frac{\mathbf{v} \cdot \hat{\mathbf{x}}_i}{aH(a)} \hat{\mathbf{x}}_i \quad (26)$$

where \mathbf{x}_i is arbitrarily chosen as one of the three coordinates and \mathbf{v} is the peculiar velocity. The density field is then created using nearest grid point (NGP) binning of the particles onto an m^3 mesh; the effect of this in Fourier space is allowed for by dividing by the normalized transform of a cubic cell,

$$J(\mathbf{k}) = \text{sinc}(\theta_x) \text{sinc}(\theta_y) \text{sinc}(\theta_z), \quad (27)$$

where $\theta_i = k_i L / 2m$.

We compute the 2D anisotropic power spectrum of both haloes and particles by binning linearly in $\mu = \cos\theta$, where θ is the angle of the wavevector to the chosen line of sight (LOS), and logarithmically in k , between the box scale mode and the Nyquist mode. We use the dimensionless redshift-space power spectrum, $\Delta^2(k, \mu)$, defined as the contribution to the redshift space variance per logarithmic interval in k and linear interval in μ

$$\sigma_s^2 = \int_{-1}^1 d\mu \int_0^\infty d \ln k \Delta_s^2(k, \mu). \quad (28)$$

Once $\Delta^2(k, \mu)$ has been computed from the particle or halo distribution we additionally compute the monopole ($\ell = 0$) and quadrupole ($\ell = 2$) moments of the full 2D distribution (e.g. Cole et al. 1994). These are given by

$$\Delta_\ell^2(k) = \frac{2\ell + 1}{2} \int_{-1}^1 P_\ell(\mu) \Delta_s^2(k, \mu) d\mu, \quad (29)$$

where $P_\ell(\mu)$ are the Legendre polynomials; $P_0(\mu) = 1$ and $P_2(\mu) = (3\mu^2 - 1)/2$. All odd moments vanish due to the symmetry $\Delta_s^2(k, \mu) = \Delta_s^2(k, -\mu)$. Almost all the redshift-space signal resides in the quadrupole, and we will concentrate on this. In order to compute the multipoles of $\Delta_s^2(k, \mu)$ we fit a model ‘monopole + quadrupole’ to $\Delta_s^2(k, \mu)$. This is necessary because this function is sampled sparsely at low k due to the finite periodic geometry of the simulation box, so that equation (29) is not well approximated by a discrete sum. Due to the orthogonality of the multipoles it is not necessary to fit a model with all (infinite) Legendre polynomials included. We always plot $\Delta_s^2(k)/k^{1.5}$ linearly in this work because at low k (box modes) the quadrupole is very noisy and can be negative, despite the Kaiser expectation.

In making estimates of power spectra from a distribution of discrete objects, it is normal to subtract shot noise:

$$\Delta^2(k) \rightarrow \Delta^2(k) - 4\pi \left(\frac{k}{2\pi}\right)^3 \frac{L^3}{N^3}, \quad (30)$$

where N^3 is the total number of objects under study. This correction is only important at small scales, and the shot noise correction has been shown to be accurate even for well-evolved glass initial conditions (Smith et al. 2003). However, we should note that this correction is inappropriate if we are purely concerned with haloes, rather than the larger number of galaxies or mass particles reconstituted from them. The shot-noise correction attempts to remove a small-scale randomness, but the locations of the haloes have a physical significance: they *are* the density field. In the halo model, the small-scale nonlinear correlations are of the form of shot noise owing to the finite numbers of haloes, softened via convolution with the halo profile. The halo-only plots in MP14 were in error in this respect, since shot noise was subtracted. But in practice the effect was small and in any case does not affect the differential comparison of models where the mass functions have been adjusted to be identical.

4.2 Models

Kaiser (1987) showed that the linear theory result for the redshift space galaxy power spectrum, $\Delta_{\text{s,g}}^2$, is given by

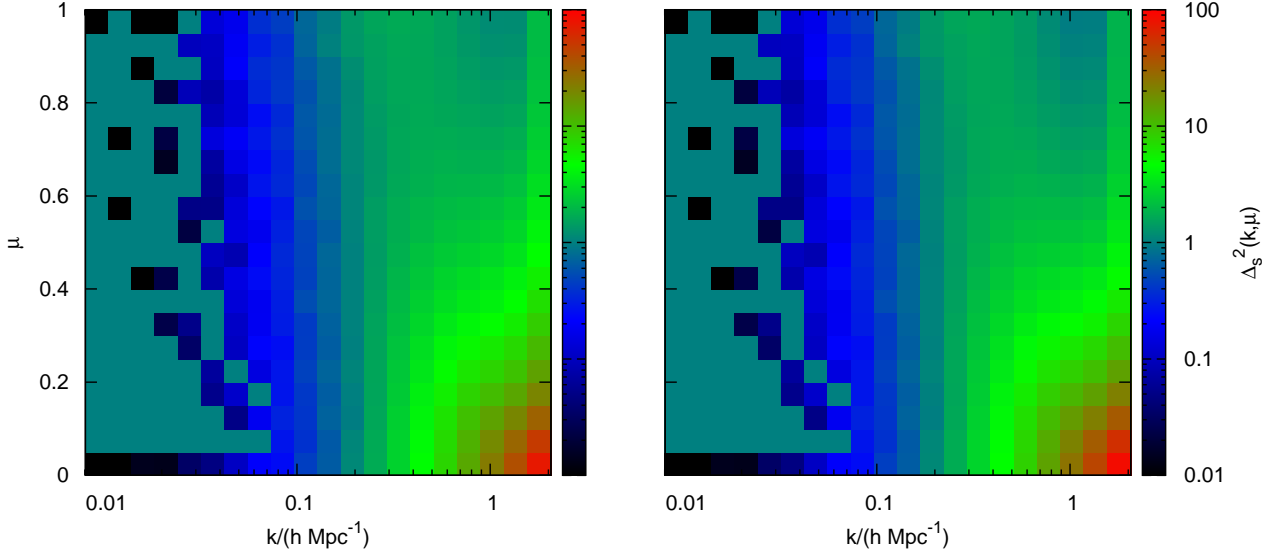


Figure 1. The redshift-space power spectrum of the full mass distribution as a function of k and μ for the rescaled simulation (left), where the AW10 method has been applied, and in addition we have restructured the internal physical and velocity structure of haloes found in the rescaled particle distribution (Section 2.2.3). This is compared to the spectrum measured in the target simulation (right). Differences in the spectra are difficult to identify visually and residuals are therefore shown in Fig. 2.

$$\Delta_{s,g}^2(k, \mu) = (b + f_g \mu^2)^2 \Delta_m^2(k) = (1 + \beta \mu^2)^2 \Delta_g^2(k), \quad (31)$$

where $\Delta_m^2(k)$ and $\Delta_g^2(k)$ the real space matter and galaxy power spectra and $\beta = f_g/b$. The growth rate features in this equation because the linear velocity field depends on the growth rate in the ZA (equation 4); this gives a universal apparent displacement to all tracers, even though their effective real-space displacements are biased in general. Expanding $\Delta_{s,g}^2(k, \mu)$ in terms of Legendre polynomials (Cole et al. 1994), the monopole and quadrupole are given by

$$\begin{aligned} \Delta_0^2(k) &= \left(1 + \frac{2}{3}\beta + \frac{1}{5}\beta^2\right) \Delta^2(k), \\ \Delta_2^2(k) &= \left(\frac{4}{3}\beta + \frac{4}{7}\beta^2\right) \Delta^2(k), \end{aligned} \quad (32)$$

and their ratio is a single function of β :

$$G(k) \equiv \frac{\Delta_2^2(k)}{\Delta_0^2(k)} \simeq \frac{1 + \frac{2}{3}\beta + \frac{1}{5}\beta^2}{\frac{4}{3}\beta + \frac{4}{7}\beta^2}. \quad (33)$$

It is infeasible to predict b with sufficient precision to convert this to the desired growth rate, but the apparent amplitude of real-space clustering can be inferred accurately, so the pure dark-matter combination $f_g \sigma_8$ can be measured.

Equation (31) is only valid on linear scales and breaks down more quickly than the linear approximation for the real-space power spectrum due to velocities becoming non-linear before densities (Scoccimarro 2004). More complicated expressions for the redshift-space power exist in the literature (e.g. Scoccimarro 2004; Taruya et al. 2010) and some prescriptions are compared by de la Torre & Guzzo (2012). These models all attempt to deal with two related issues: (1) deviations of the real-space power spectrum from linear theory; (2) additional sources of anisotropy beyond the bare Kaiser model. The latter effects amount to more rapid damping of modes that lie close to the line of sight (e.g. Kwan et al. 2012), known under the generic title of ‘fingers-of-God’ (FOG), since this damping amounts to a radial convolution in configuration space. A common simple model

displaying both these effects is the ‘Kaiser+Lorentzian’ (Peacock & Dodds 1994), in which the nonlinear power spectrum is subject to the Kaiser anisotropy and a radial damping controlled by the pairwise dispersion σ :

$$\Delta_s^2(k, \mu) = \frac{(b + f_g \mu^2)^2 \Delta_{NL}^2(k)}{1 + k^2 \sigma^2 \mu^2 / 2}. \quad (34)$$

In practice, there are two distinct sources of FOG effects: pure quasi-linear terms (which can be estimated e.g. via the ZA), plus the internal velocity dispersion of haloes. In our modelling, the first kind of FOG should be included directly, since we work with a dynamically realistic halo catalogue. But the internal velocity dispersions are an important contributors to the overall effect, and we need to understand the effect on these of internal halo rescaling.

5 RESULTS OF RESCALING

5.1 Enhanced AW10 approach

We now show a number of examples of the effect of rescaling on the redshift-space power spectrum. We begin with the original AW10 method applied to a full particle distribution, with additional restructuring of internal halo properties as in Section 2.2.3. The full redshift space power spectrum before and after scaling is shown in Fig. 1 where differences in the power between the rescaled and target simulation are difficult to see by eye. Residuals are therefore shown in Fig. 2 together with the monopole and quadrupole moments. The monopole is very well reproduced (at the 1% level up to $k = 0.1 h \text{ Mpc}^{-1}$), including good recovery of the BAO feature from the large-scale displacement step, as in the case of real space. Deviations are seen at smaller scales if no changes are made to the internal structure of haloes. Improvements are gained either by restructuring the haloes or by replacing them entirely. To reconstitute haloes of a given mass we assigned halo virial radii according to equation (16), took

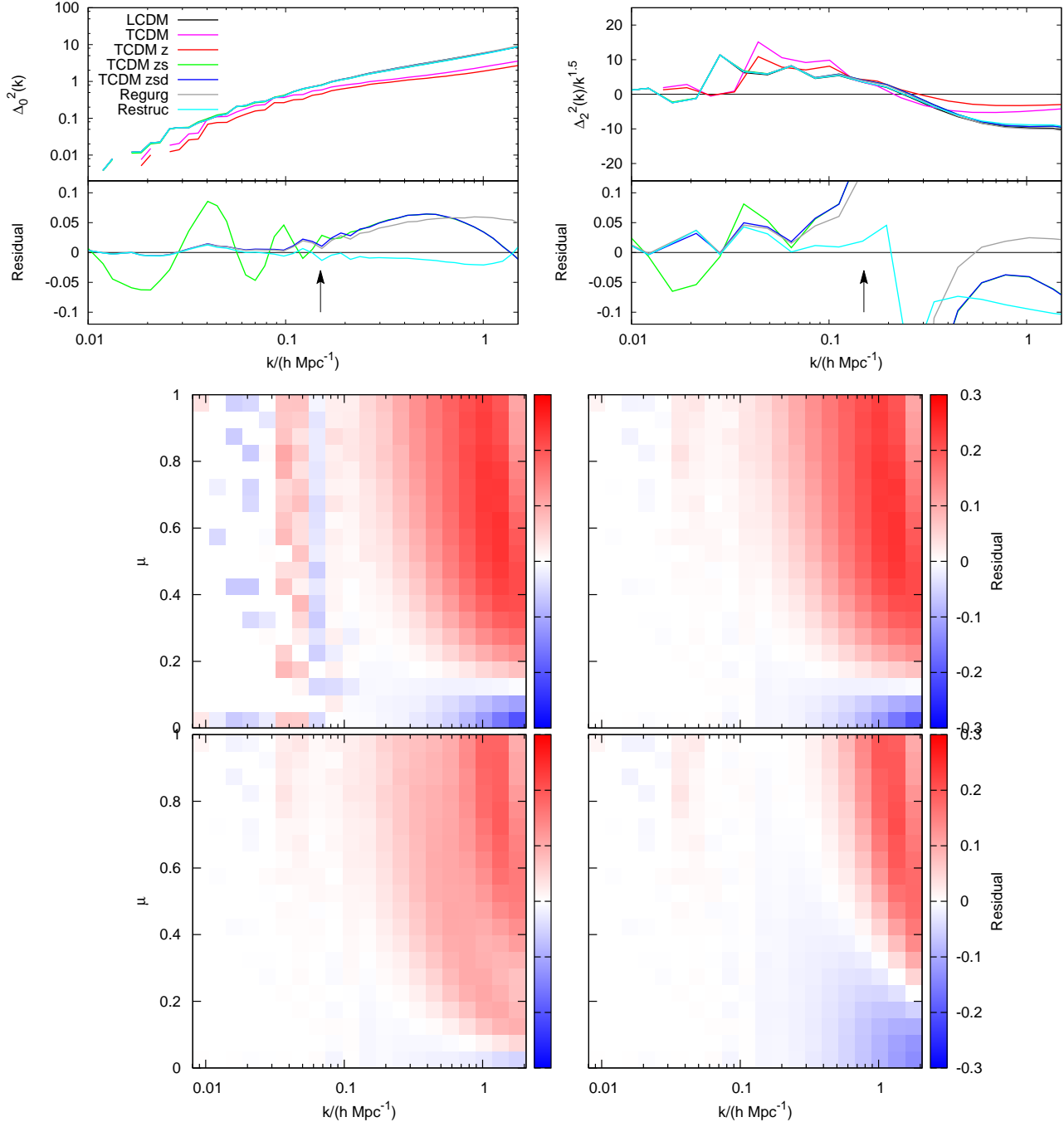


Figure 2. Redshift-space results for a rescaled particle distribution, using the original AW10 method supplemented by various alterations of halo internal structure. The upper two panels show the monopole (left) and quadrupole (right) power spectra with the arrow showing the non-linear scale. The monopole is accurate to 3% to $k = 1 h \text{ Mpc}^{-1}$ if the restructuring method is used, including good reproduction of the BAO feature via the displacement field correction. The quadrupole is less well reproduced with errors at the 5% level at large scales, but clearly applying the displacement field step of the method improves the match, and restructuring extends the match to quasi-linear scales ($k \simeq 0.2 h \text{ Mpc}^{-1}$). At non-linear scales it is regurgitation that performs better. The lower four panels show the fractional residuals for the full redshift-space power spectrum at each stage of the rescaling process when compared to the target ΛCDM simulation. The middle left panel shows the scaling in redshift and size and the middle right panel shows the addition of the displacement field step. The bottom left panel then shows the effect of removing haloes and regurgitating haloes with theoretical velocity dispersions back into the parent particle distribution; the bottom right panel shows the effect of restructuring haloes. Regurgitation and restructuring haloes perform slightly different in the non-linear portions of redshift space. It is clear from this plot that the good agreement of the restructuring monopole is partially due to cancellations of errors across the full redshift-space plane.

concentrations from the Bullock et al. (2001) relations and assigned Gaussian velocity dispersions from equation (19). Haloes were created in an aspherical manner, as described in Section 2, although we found that the asphericity mattered very little at the level of the redshift-space power.

In contrast to the case of real space, shown in Fig. 8 of MP14, restructuring haloes performs better than regurgitation when compared in redshift space. Looking at the ratios to the target in the full redshift-space power information, shown in Fig. 2, one can see that regurgitation performs better for perpendicular modes that are unaffected by redshift distortions, but that restructuring performs slightly better across all modes, accounting for the slightly better overall prediction for the monopole. The eventual monopole in the restructured case is good to 3% up to $k = 1 h \text{ Mpc}^{-1}$, whereas the regurgitated monopole is good to 5%. The quadrupole is noisier and 5% deviations can be seen up to the non-linear scale where the fractional error blows up as the quadrupole changes sign. However, it is still evident that the displacement field step of the method provides a better quadrupole at large scales.

5.2 Rescaling halo catalogues

We now turn to the results of rescaling the halo catalogues directly. Fig. 3 compares the redshift-space power of the rescaled halo distribution to that of the target haloes. As in real space, the original AW10 method fails to handle the BAO feature correctly until haloes are given mass-dependent additional displacements. But the error is smaller in redshift space, because the additional velocity field does not depend on halo mass. The agreement in the monopole power is around 5% for the full halo sample out to $k = 1 h \text{ Mpc}^{-1}$, but contains a slant which is shot noise due to the numbers of haloes not being perfectly matched (recall that the mass functions still differ at the 10% level post scaling). Note that although the non-linear scales have not been modified here the match is still reasonable due to the lack of an internal velocity induced FOG in the halo distribution. However, the rescaled quadrupole is significantly less accurate than the monopole, with residuals at the 10% level. Moreover, there is some suggestion of a remaining large-scale residual that correlates with the BAO signal, of amplitude about 5% and there are some large deviations at large scales. Additionally the displacement field step of the method seems to improve matters only marginally.

5.3 Reconstituted haloes

We now show the results of reconstituting haloes by modifying the positions and velocities of the halo particles. It is illuminating to test this aspect of our approach directly in an unscaled simulation (the $L = 780 h^{-1} \text{ Mpc}$ ΛCDM simulation discussed in Section 3). We show the redshift-space monopole, quadrupole and the full 2D redshift-space power spectrum in Fig. 4. In both figures we compare results using reconstituted halo particles to the ‘exact’ results based on the particles from which the halo catalogue was constructed. This tests our assumptions about both the halo internal physical and velocity structure. Haloes were reconstructed with NFW profiles (equation 15) with concentrations from Bullock et al. (2001) and velocity dispersion was

assumed to be Gaussian with a standard deviation given by equation (19). The agreement in the monopole is almost perfect (within 1% up to $k = 1 h \text{ Mpc}^{-1}$) if catalogued velocity dispersions are used, but deviations occur when using a theoretically predicted σ_v , which predicts too high a power, suggesting that σ_v is too low and FOG are not strong enough. This can be seen via a direct comparison of predicted and catalogued dispersions, which show the predicted value to be low by a factor of 1.07. According to equation (16), such a factor would arise if the virialized overdensity threshold was raised to about $\Delta_v \simeq 300$. We note that an increased Δ_v is consistent with spherical model predictions for ΛCDM models (e.g. Bryan & Norman 1998) but is incompatible with our choice of $b = 0.2$ as a linking length. We have not pursued the possibility of changing Δ_v as we do not want to introduce free parameters that may have an unknown dependence on cosmology or simulation resolution (e.g. Power & Knebe 2006; Smith et al. 2014).

Finally in Fig. 5 the redshift-space power of particles in reconstituted haloes is compared to that of particles in haloes in the target cosmology. The agreement is good at linear scales once a biased displacement field has been used. At non-linear scales the agreement is less good if one uses the theoretical dispersion relation in equation (19) compared to using a rescaled version of the catalogued halo velocity dispersion; in the later case the eventual agreement for the monopole is impressive and is at the 3% level across all scales shown. Although the quadrupole has a larger error, this still remains within 5% in regions where it is not passing through zero. In 2D redshift space one can see that large fractional errors in the catalogued dispersion case are concentrated at high k and high μ ; these contribute less to the monopole because the full power is damped here and the monopole is a simple average. Using theoretical dispersions perform worse across the entirety of redshift space, even at surprisingly large scales for high μ . This plot, combined with the tests in Fig. 4 gives hope that the theoretical dispersion relation could be modified slightly to produce better results. We have not pursued this here as our aim was to see how far one could get without resorting to tuning additional parameters.

5.4 Recovery of the growth rate

A realistic goal of forthcoming galaxy redshift surveys will be to measure the growth rate of cosmic structure with $\sim 1\%$ accuracy (e.g. *DESI*, *Euclid*). Can such a precision be attained via simulations that have undergone rescaling? Fig. 6 shows the recovered $G(k) = \Delta_2^2(k)/\Delta_0^2(k)$ ratio for: the full rescaled particle distribution; the rescaled halo distribution; the distribution of particles in haloes reconstituted from halo catalogues.

At large scales for the case of the full matter distribution all approaches are accurate to around 5% out to $k = 0.1 h \text{ Mpc}^{-1}$. If haloes are restructured this accuracy is extended out to $k = 0.2 h \text{ Mpc}^{-1}$. For the case of both the haloes and halo particles large deviations are seen at the largest scales which remedy themselves to the 7% level for haloes, and 5% level for halo particles, out to the non-linear scale.

In each plot the linear theory G_{lin} is shown (equation 33); for the full matter distribution $G_{\text{lin}} \simeq 0.55$. and for the haloes, we expect $G_{\text{lin}} \simeq 0.37$ or 0.28 for respectively

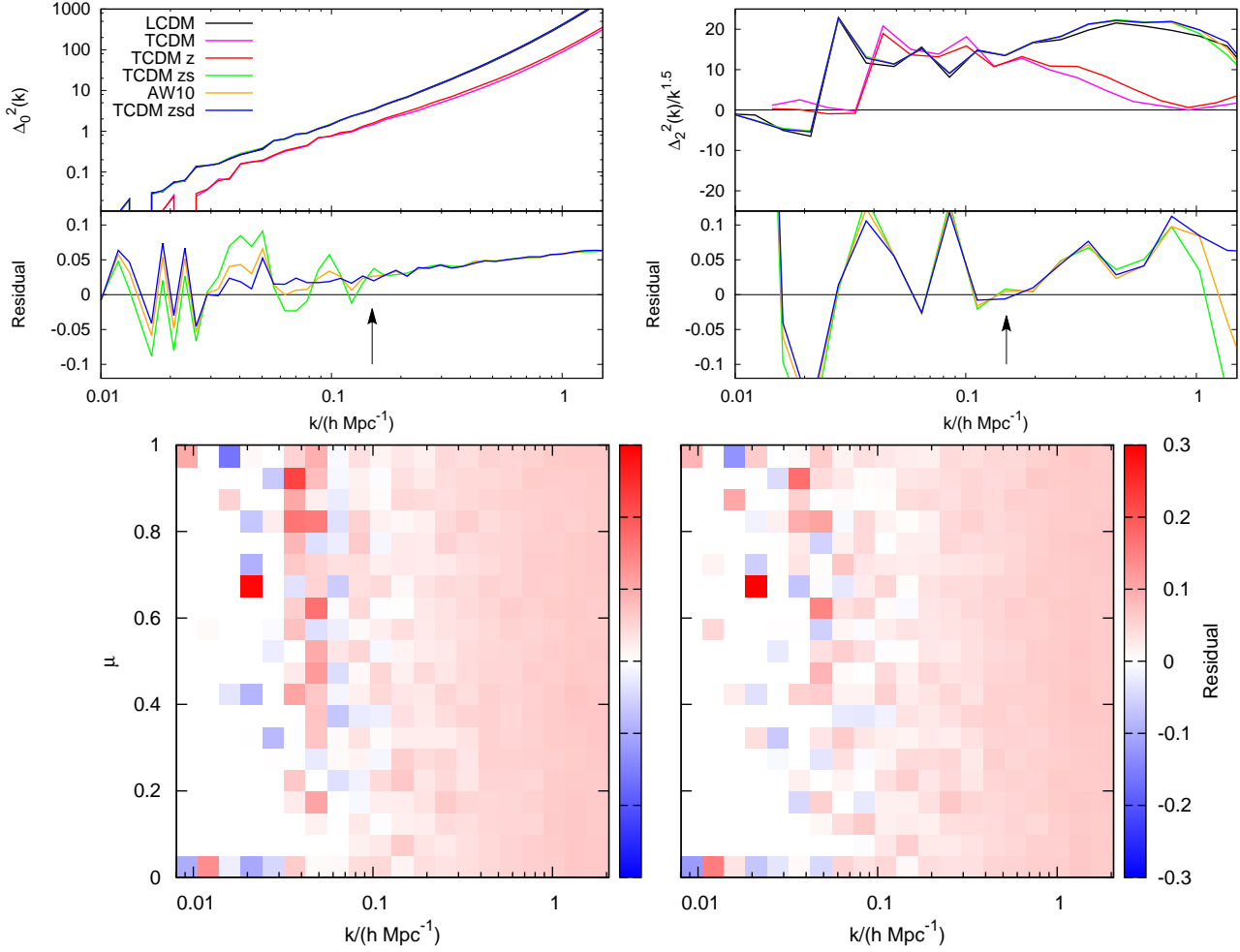


Figure 3. The upper two panels show the halo redshift-space monopole (left) and quadrupole (right) power at each stage of the scaling with the arrow denoting the non-linear scale. The monopole is recovered at the few % level across all scales, but the match surprisingly degrades somewhat at large scales. As in MP14 applying a biased displacement field (*zsd*) to haloes outperforms the original AW10 method (AW10). The slant is shot noise due to differing halo numbers, which arises due to the slightly imperfect match for the halo mass function. The quadrupole is only recovered at the 10% level and contains large residuals that are only very slightly remedied by the displacement field correction. The lower panels show the fractional residuals of the 2D redshift-space power spectrum of the original to target simulations after scaling in box size and redshift (bottom left; equivalent to *zs* curve) and after additionally applying a biased displacement field correction, and a velocity field correction, to halo positions (bottom right; equivalent to *zsd* curve). The match is improved by applying the displacement and velocity field correction in the final stage of the method. The match is reasonable at small scales because there are no strongly non-linear FOG effects in the halo distribution.

the equal-weighted and mass-weighted cases (taking into account the effective bias discussed in Section 2). Fig. 6 indicates that the rescaled simulations are consistent with these growth rates but that large deviations are seen around the box scale, although in the case of haloes a simulation containing larger scales (thus more linear modes) would help to support this conclusion.

At smaller scales, the results are most satisfactory in the case of the halo distribution, where the error in the quadrupole-to-monopole ratio is relatively flat, at typically around 4%. There are occasional spikes to higher values, but these are unlikely to disrupt the recovery of the growth rate at this typical error rate. Conversely, the results for the overall mass are less impressive, with errors exceeding 5% for a broad band of wavenumbers beyond the non-linear scale. Fortunately, this case is not of practical interest, whereas we are most concerned with particles in haloes as

a simple proxy for a galaxy catalogue. Here, the last panel in Fig. 6 shows that usefully precise results to wavelengths large enough to extract most of the cosmological information ($k \simeq 0.3 h \text{ Mpc}^{-1}$) would require improved treatment of the internal halo velocity dispersion, with the rescaled values and pure theoretical values bracketing the truth.

In a practical survey analysis one could marginalize over velocity dispersion nuisance parameters, but this would diminish the statistical power of the high- k data. Some encouragement comes from the fact that the non-linear portion of $G(k)$ for haloes is particularly well matched, which is related to the fact that they lack a strongly non-linear FOG. It is plausible that future surveys may attempt to target only halo central galaxies in order to mitigate the effect of FOG in this way, or to use other weighting schemes (e.g. Seljak et al. 2009).

In any case, the example illustrated here undoubtedly

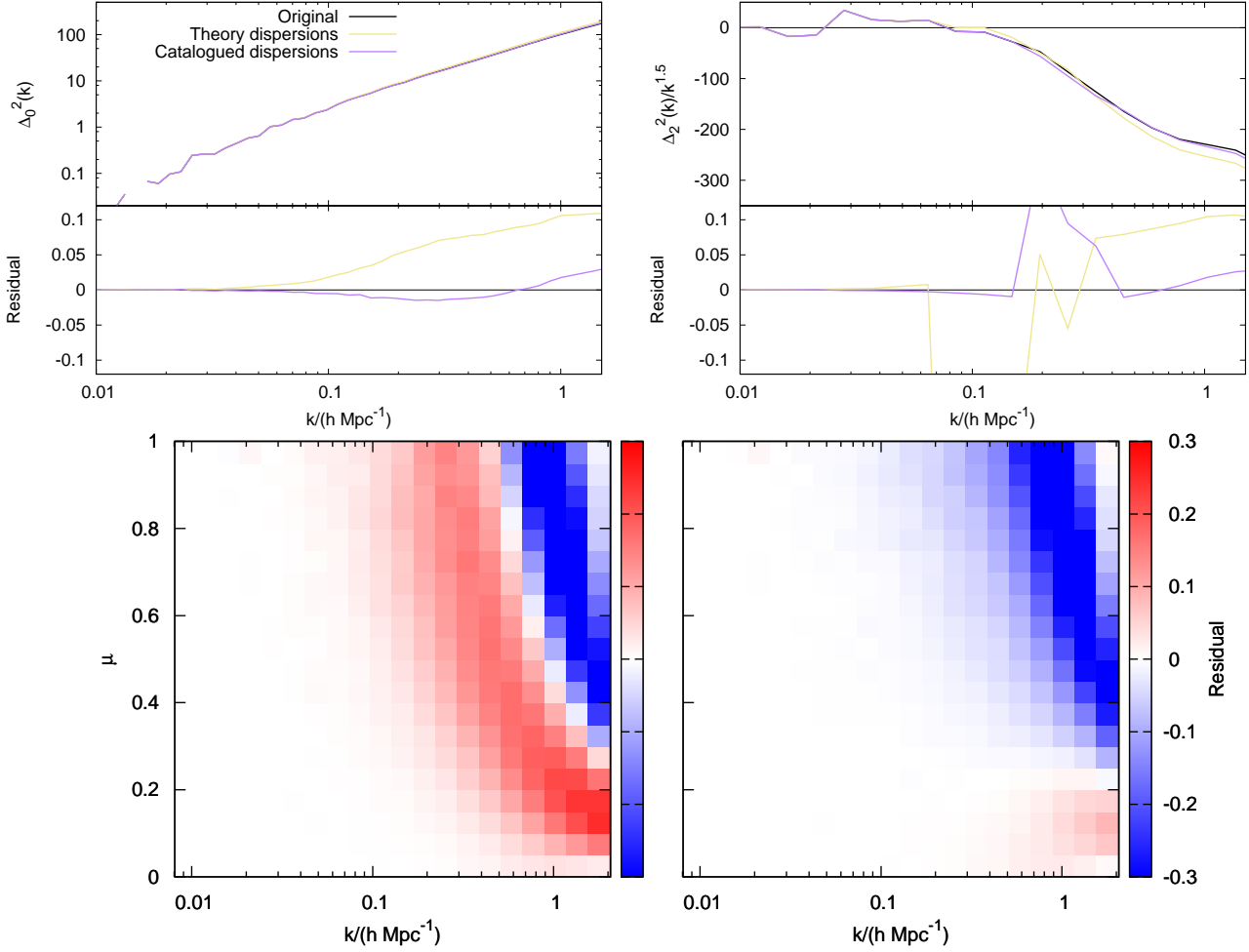


Figure 4. A comparison of the power spectra of particles in haloes reconstituted from a halo catalogue, compared to the original simulation particles in the haloes. The upper panels show the monopole (left) and quadrupole (right) power while the lower two panels show the fractional residuals for the full redshift-space power spectrum as function of k and μ in the case when haloes are assigned velocity dispersions using equation (19; left; equivalent to ‘theory’ curve above) as compared with the measured velocity dispersions (right; equivalent to ‘catalogue’ curve above). The error in the quadrupole blows up around $k = 0.1 h \text{ Mpc}^{-1}$ where the quadrupole power changes sign. Using the catalogued value of the dispersions produces more accurate results, with the reconstituted monopole being almost perfectly reproduced (within $\simeq 1\%$) up to $k = 1 h \text{ Mpc}^{-1}$. The lower panels show that the error from using the predicted dispersion differs across redshift space and extends to larger scales than that from using the catalogued dispersions. The monopole from using catalogued dispersions is recovered well because errors here are concentrated in the high- μ -high- k region of the plane where the absolute magnitude of the power is low due to FOG. This means that the monopole is relatively unaffected but this is less true of the quadrupole, which differences in μ . The match is perfect at large scales in all cases because the haloes are placed perfectly accurately by construction.

makes greater demands on the method than would be encountered in most practical applications, where the range of parameter space to be spanned would consist of models that are closer to Λ CDM. The above errors would undoubtedly decline in proportion to the distance between models in parameter space. This in itself could create new problems: if the degree of rescaling is very small, then there will be little chance of finding an output at an input redshift z suitable to match a desired target z' . Instead, we may have to accept that the original simulation defines a grid in z' for the target cosmology, over which we have no choice. But provided the outputs are reasonably well spaced, this need not be a problem: construction of a light-cone mock galaxy sample from HOD galaxies populating the snapshots would

proceed in much the same way, independent of the exact set of z' values.

6 SUMMARY AND CONCLUSIONS

In this paper we have considered the rescaling of simulated dark-matter haloes in order to create catalogues of haloes that are characteristic of an altered cosmological model, focusing on the behavior of the method in redshift space. This extends our previous work in real space (Mead & Peacock 2014; MP14), which was based on the original proposal of Angulo & White (2010; AW10). MP14 demonstrated that rescaling of simulations could be made to work in real space directly from halo catalogues, without needing to manipu-

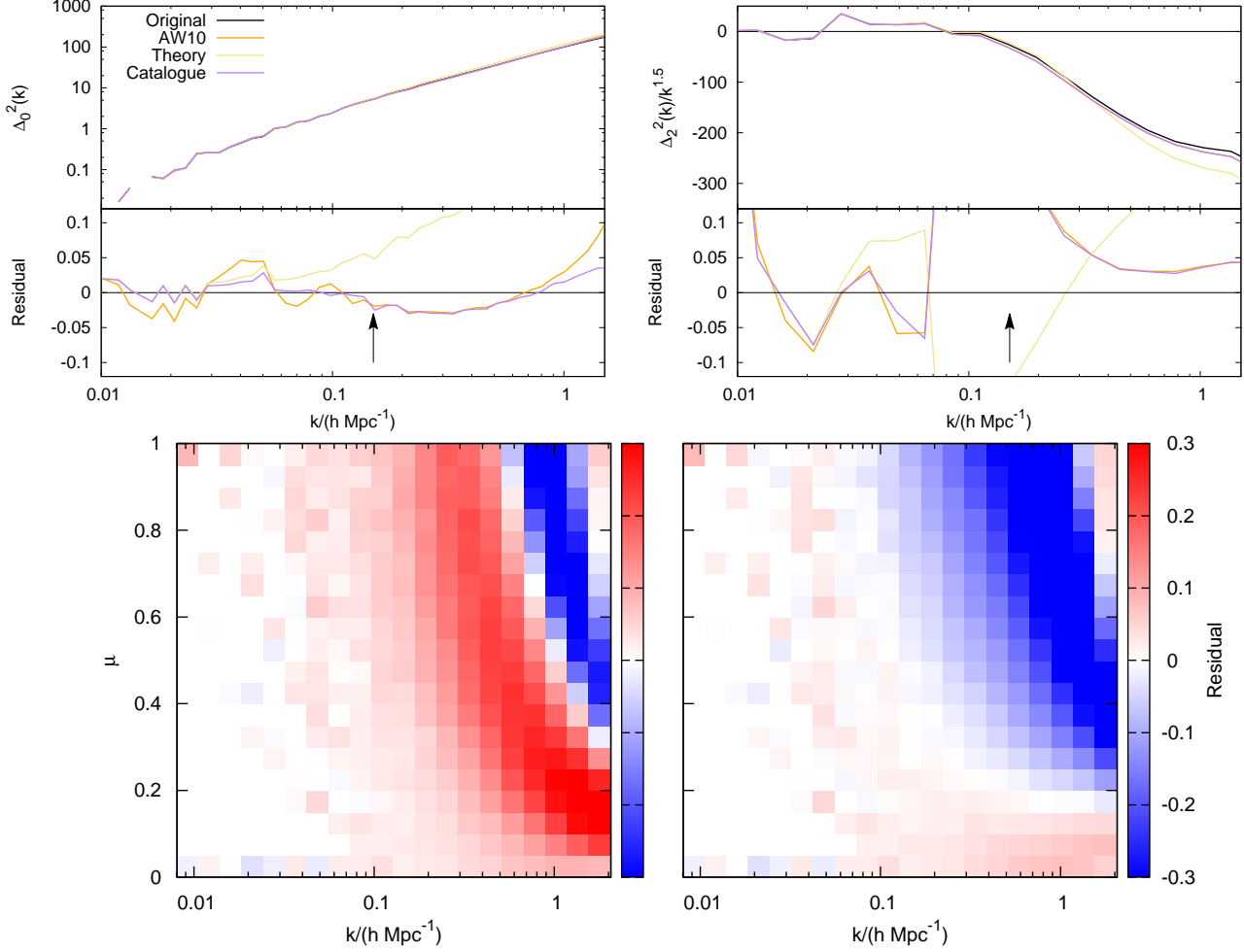


Figure 5. The upper two panels show the monopole (left) and quadrupole (right) power spectra of particles in reconstituted haloes compared to particles in haloes in the target simulation. If the original AW10 method is used (AW10) and haloes are reconstituted with catalogued halo velocity dispersions a large residual BAO feature is seen up to the non-linear scale (arrow), which is removed if a biased displacement field is used as in the other two curves. In these two cases better results are obtained for the monopole and quadrupole if rescaled catalogued dispersions are used (catalogue) compared to theoretical dispersions (theory). However, the quadrupole is relatively insensitive to the method used in the scaling and shows a larger error which remains at the 5% level on linear scales. The fractional residuals of the full redshift-space power spectrum is shown in the lower two panels from using biased displacements together with theoretical velocity dispersions (left, equivalent to ‘theory’ curves above) and rescaled catalogued dispersions (right, equivalent to ‘catalogue’ curves above). Errors in the catalogued case are concentrated at high k and high μ , where there is less overall power, resulting in a better recovery of the monopole and quadrupole.

late the full particle data. In addition to the resulting advantage in speed and storage, this approach also allows improvements over AW10 in terms of the dependence of bias on halo mass and the small-scale clustering, which is affected by internal changes to halo structure.

For these reasons, it is clearly of interest to see if the MP14 approach also works acceptably in redshift space, allowing it to be used as the basis for a complete approach to the construction of simulated surveys. We have therefore carried out the extreme test of rescaling a halo catalogue generated from a matter-only τ CDM simulation into that of a more standard Λ CDM model. In redshift space the MP14 method works well at the level of the monopole, as in the original AW10 case. For the full particle distribution the redshift-space monopole was recovered at the 2% level up to $k = 0.1 h \text{ Mpc}^{-1}$ and to 3% to smaller scales if halo internal properties are also manipulated. Rescaling also worked

well when applied to haloes in redshift space, although the improvements gained from using a biased displacement field are less marked because redshift space mixes in the unbiased velocity field. The monopole agrees at the few % level out to $k = 1 h \text{ Mpc}^{-1}$, although the numerical results show some deviations at the very largest scales investigated and the origin of these is not known. For reconstituted haloes, the monopole power spectrum was recovered at the 1% level up to $k = 0.1 h \text{ Mpc}^{-1}$ if a biased displacement field is used and the agreement is at the 3% level up to $k = 1 h \text{ Mpc}^{-1}$ if catalogued dispersions are also rescaled.

The quadrupole to monopole ratio, $G(k)$, is of especial interest because it can be used in the linear regime to infer the growth rate of cosmic structure. We found that this could be recovered at the typical level of around 5% for haloes themselves, even out to wavenumbers as high as $k = 1 h \text{ Mpc}^{-1}$. This is most encouraging given how far our

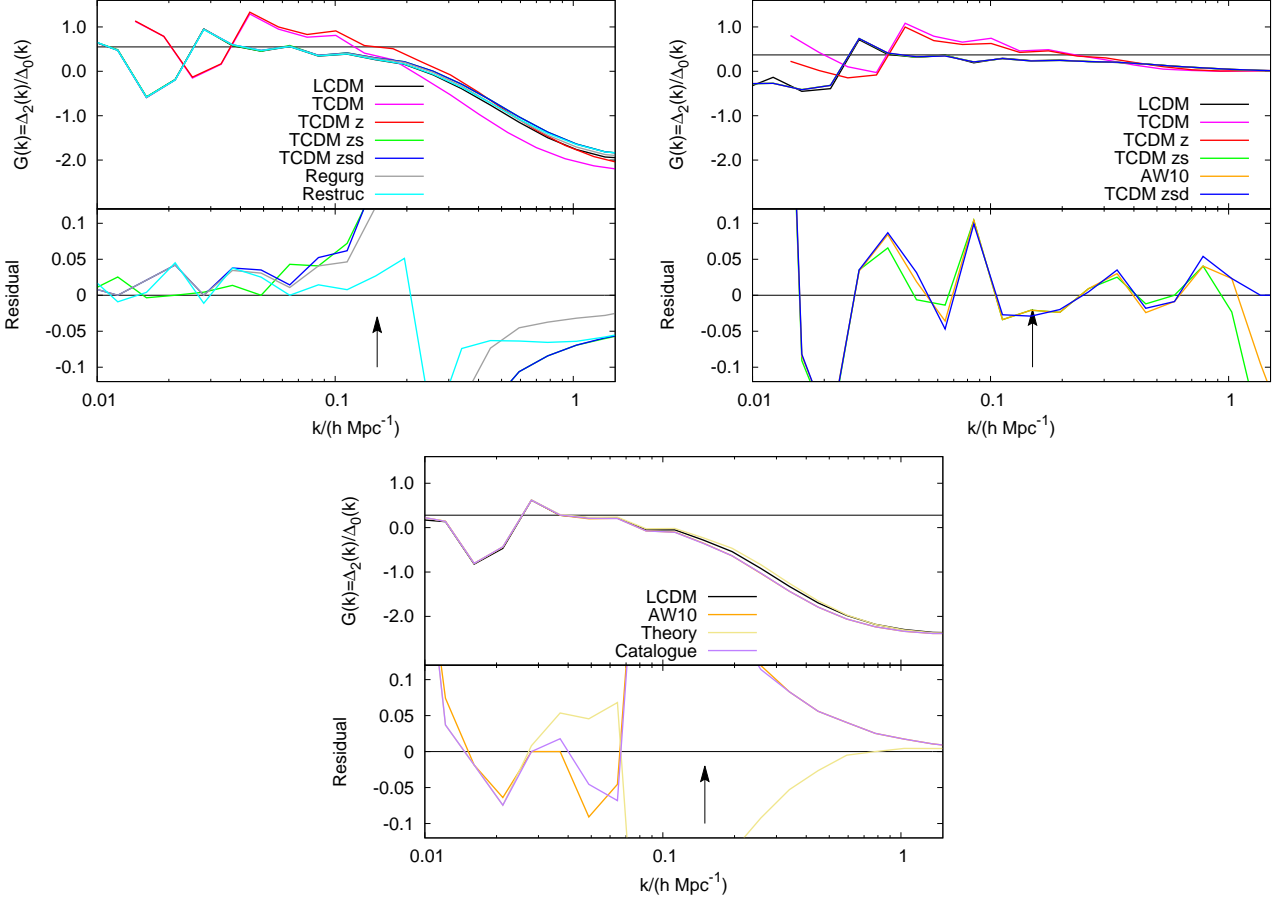


Figure 6. The value of $G(k) = \Delta_2^2(k)/\Delta_0^2(k)$ recovered from the simulations before and after scaling. In each case the non-linear scale is shown with an arrow. The top left panel shows the case of the full particle distribution where methods of regurgitation and restructuring have been used to alter halo interiors. Here the residual difference is small across the full range of scales, and is at the 5% level on linear scales, with the non-linear tail being reproduced at the 5% level by all methods, in the region where the quadrupole is not passing through zero. The full range of scales is best matched by the restructuring method. The top right panel shows the case of haloes themselves, whereas the bottom panel shows the case of reconstituted halo particles with both theoretical and catalogued velocity dispersions used in the reconstitution, in both cases a comparison is made with the original AW10 method, which performs well here because the residual BAO is effectively divided out and with it the error due to a slightly incorrect $b(M)$ relation. For haloes the value of $G(k)$ is reproduced at the 10% level across all scales and when the halo particles are considered the match is at the 5% level when the quadrupole is not passing through zero and the non-linear tail is fairly well recovered in this case.

input τ CDM model is from anything close to Λ CDM, and it suggests that the required 1% precision should readily be obtained for models that are allowed by existing cosmological constraints.

But for particles in haloes (an example of a galaxy HOD, albeit an unrealistic one), the high- k precision in $G(k)$ is considerably poorer, reflecting the difficulty in achieving an appropriate level for the internal halo velocity dispersions using simple scaling recipes. Again this problem will diminish (at least in the case of rescaling ‘observed’ dispersions) as the input model approaches closer to the target. There are several routes by which the modelling of the halo-particle power spectrum may be improved – either via more sophisticated dynamical modelling of the halo velocity dispersion, or via weighting schemes that suppress this component of the FOG. We therefore see the current results as giving encouragement that halo rescaling will be a practically useful modelling method in the era when data on redshift-space distortions reaches the 1% level.

ACKNOWLEDGEMENTS

AJM acknowledges the support of an STFC studentship and support from the European Research Council under the EC FP7 grant number 240185.

REFERENCES

- Anderson L. et al., 2014, MNRAS, 439, 83
- Angulo R. E., White S. D. M., 2010, MNRAS, 405, 143
- Bryan G. L., Norman M. L., 1998, ApJ, 495, 80
- Bullock J. S., Kolatt T. S., Sigad Y., Somerville R. S., Kravtsov A. V., Klypin A. A., Primack J. R., Dekel A., 2001, MNRAS, 321, 559
- Cole S., Fisher K. B., Weinberg D. H., 1994, MNRAS, 267, 785
- Cooray A., Sheth R., 2002, Physics Reports, 372, 1
- Davis M., Efstathiou G., Frenk C. S., White S. D. M., 1985, ApJ, 292, 371

- de la Torre S., Guzzo L., 2012, *MNRAS*, 427, 327
- de la Torre S. et al., 2013, *A&A*, 557, A54
- Dooley G. A., Griffen B. F., Zukin P., Ji A. P., Vogelsberger M., Hernquist L. E., Frebel A., 2014, *ApJ*, 786, 50
- Eisenstein D. J., Seo H.-J., Sirko E., Spergel D. N., 2007, *APJ*, 664, 675
- Eke V. R., Cole S., Frenk C. S., 1996, *MNRAS*
- Eke V. R., Navarro J. F., Steinmetz M., 2001, *ApJ*, 554, 114
- Guo Q., White S., Angulo R. E., Henriques B., Lemson G., Boylan-Kolchin M., Thomas P., Short C., 2013, *MNRAS*, 428, 1351
- Kaiser N., 1987, *MNRAS*, 227, 1
- Kazantzidis S., Magorrian J., Moore B., 2004, *ApJ*, 601, 37
- Kwan J., Lewis G. F., Linder E. V., 2012, *ApJ*, 748, 78
- Lacey C., Cole S., 1993, *MNRAS*, 262, 627
- Li B., Efstathiou G., 2012, *MNRAS*, 421, 1431
- Lukić Z., Heitmann K., Habib S., Bashinsky S., Ricker P. M., 2007, *ApJ*, 671, 1160
- Mead A. J., Peacock J. A., 2014, *MNRAS*, 440, 1233
- Merritt D., Graham A. W., Moore B., Diemand J., Terzić B., 2006, *AJ*, 132, 2685
- Merritt D., Navarro J. F., Ludlow A., Jenkins A., 2005, *ApJL*, 624, L85
- Moore B., Quinn T., Governato F., Stadel J., Lake G., 1999, *MNRAS*, 310, 1147
- Navarro J. F., Frenk C. S., White S. D. M., 1997, *ApJ*, 490, 493
- Neto A. F. et al., 2007, *MNRAS*, 381, 1450
- Padmanabhan N., Xu X., Eisenstein D. J., Scalzo R., Cuesta A. J., Mehta K. T., Kazin E., 2012, *MNRAS*, 427, 2132
- Peacock J. A., Dodds S. J., 1994, *MNRAS*, 267, 1020
- Peacock J. A., Smith R. E., 2000, *MNRAS*, 318, 1144
- Percival W. J., 2005, *A&A*, 443, 819
- Power C., Knebe A., 2006, *MNRAS*, 370, 691
- Press W. H., Schechter P., 1974, *ApJ*, 187, 425
- Rasera Y., Alimi J.-M., Courtin J., Roy F., Corasaniti P.-S., Füzfa A., Boucher V., 2010, in *American Institute of Physics Conference Series*, Vol. 1241, *American Institute of Physics Conference Series*, Alimi J.-M., Fuözfa A., eds., pp. 1134–1139
- Reed D. S., Bower R., Frenk C. S., Jenkins A., Theuns T., 2007, *MNRAS*, 374, 2
- Ruiz A. N., Padilla N. D., Domínguez M. J., Cora S. A., 2011, *MNRAS*, 418, 2422
- Samushia L. et al., 2013, *MNRAS*, 429, 1514
- Schmidt F., Lima M., Oyaizu H., Hu W., 2009, *Phys. Rev. D*, 79, 083518
- Scoccimarro R., 2004, *Phys. Rev. D*, 70, 083007
- Seljak U., 2000, *MNRAS*, 318, 203
- Seljak U., Hamaus N., Desjacques V., 2009, *Physical Review Letters*, 103, 091303
- Seljak U., Zaldarriaga M., 1996, *ApJ*, 469, 437
- Sheth R. K., Mo H. J., Tormen G., 2001, *MNRAS*, 323, 1
- Sheth R. K., Tormen G., 1999, *MNRAS*, 308, 119
- Simha V., Cole S., 2013, *MNRAS*, 436, 1142
- Smith R. E., Desjacques V., Marian L., 2011, *Phys. Rev. D*, 83, 043526
- Smith R. E. et al., 2003, *MNRAS*, 341, 1311
- Smith R. E., Reed D. S., Potter D., Marian L., Croce M., Moore B., 2014, *MNRAS*, 440, 249
- Spergel D. N. et al., 2003, *ApJs*, 148, 175
- Springel V., 2005, *MNRAS*, 364, 1105
- Springel V. et al., 2005, *Nature*, 435, 629
- Taruya A., Nishimichi T., Saito S., 2010, *Phys. Rev. D*, 82, 063522
- Taylor A., Joachimi B., Kitching T., 2013, *MNRAS*, 432, 1928
- Tinker J., Kravtsov A. V., Klypin A., Abazajian K., Warren M., Yepes G., Gottlöber S., Holz D. E., 2008, *ApJ*, 688, 709
- Wojtak R., Lokas E. L., Gottlöber S., Mamon G. A., 2005, *MNRAS*, 361, L1
- Zel'dovich Y. B., 1970, *A&A*, 5, 84
- Zheng Z. et al., 2005, *ApJ*, 633, 791